Rapid Communications

Second harmonic generation as a probe of broken mirror symmetry

Bryan T. Fichera,[1] Anshul Kogar,[1] Linda Ye,[1] Bilal Gökce,[1,2] Alfred Zong,[1] Joseph G. Checkelsky,[1] and Nuh Gedik[1,*]

[1]*Department of Physics, Massachusetts Institute of Technology, Cambridge, Massachusetts 02139, USA*

[2]*Technical Chemistry I and Center for Nanointegration Duisburg-Essen (CENIDE), University of Duisburg-Essen, 45141 Essen, Germany*

(Received 29 July 2019; revised manuscript received 25 February 2020; accepted 21 May 2020; published 8 June 2020)

The notion of spontaneous symmetry breaking has been used to describe phase transitions in a variety of physical systems. In crystalline solids, the breaking of certain symmetries, such as mirror symmetry, is difficult to detect unambiguously. Using $1T$-TaS_2, we demonstrate here that rotational-anisotropy second harmonic generation (RA-SHG) is not only a sensitive technique for the detection of broken mirror symmetry, but also that it can differentiate between mirror symmetry-broken structures of opposite planar chirality. We also show that our analysis is applicable to a wide class of different materials with mirror symmetry-breaking transitions. Lastly, we find evidence for bulk mirror symmetry-breaking in the incommensurate charge density wave phase of $1T$-TaS_2. Our results pave the way for RA-SHG to probe candidate materials where broken mirror symmetry may play a pivotal role.

DOI: 10.1103/PhysRevB.101.241106

In condensed matter systems, phases are often classified by the symmetries that they break. Identifying these symmetries enables one to understand a system's order parameter, collective excitations, topological defects, and allowable topological indices [1,2]. Together, these attributes allow one to predict how a material will respond to external perturbations like electromagnetic fields, heat, and mechanical forces, which is a central goal of condensed matter physics.

Specifically, the presence or absence of mirror symmetry can lead to a variety of unusual phases and properties. For example, the absence of mirror plane symmetry in noncentrosymmetric materials can give rise to gyrotropic order, which can lead to a nonzero out-of-plane circular photogalvanic effect [3]. Moreover, in certain topological crystalline insulators, such as SnTe, the presence of mirror symmetry can give rise to conducting surface states through the existence of a nonzero mirror Chern number. This topological index guarantees an even number of Dirac cones on surfaces where mirror symmetry is retained [4–6].

In other circumstances, like that in the pseudogap regime of cuprate superconductors, the existence of mirror symmetry is more controversial and has led some to seek an experimental method to serve as a binary indicator of broken mirror symmetry [7]. In principle, several tools can already do this, including resonant ultrasound spectroscopy [8,9], x-ray, neutron, and electron diffraction [10,11], and a recently proposed method, shear conductivity [7]. Resonant ultrasound spectroscopy and the diffraction-based techniques are more sensitive to the ionic lattice, which makes the identification of subtle electronic symmetry-breaking challenging. And while shear conductivity has the potential to be an extremely versatile tool for identifying broken point group symmetries, experimental pursuits are currently only preliminary [7]. In this study, we focus on a nonlinear optical technique, rotational-anisotropy second harmonic generation (RA-SHG), which we show is capable not only of identifying broken mirror symmetry [12] but also of resolving its sense (left- or right-handed). Furthermore, RA-SHG is sensitive to the electronic subsystem and can be used for microscopy studies, making it an ideal experimental tool for probing phase transitions where domains may arise [13,14].

In this direction, we choose a material, $1T$-TaS_2, in which vertical mirror plane symmetry is manifestly broken across an incommensurate (IC) to nearly commensurate (NC) charge density wave (CDW) transition [15,16]. Using this material, we demonstrate in this Rapid Communication that RA-SHG is an effective probe of broken mirror symmetry. We also show that the sense (i.e., left- or right-handed) associated with the mirror symmetry-broken structure is encoded in the angular dependence of the RA-SHG signal. Thus, RA-SHG can be used to differentiate mirror-opposite domains. While the data presented in this work is specific to the case of $1T$-TaS_2, we also show analytically that our technique is applicable to a wide class of transitions involving spontaneously broken mirror symmetry.

$1T$-TaS_2 is a layered material with a crystallographic structure identical to other octahedrally coordinated transition metal dichalcogenides [Fig. 1(a)]. The space group of the high temperature, undistorted phase is $P\bar{3}m1$ (No. 164, point group D_{3d}) [17], and the point group of the surface normal to the (001) direction in this phase is C_{3v} [18,19]. Upon lowering temperature, $1T$-TaS_2 undergoes a series of CDW transitions. At $T_{IC} = 550\,K$, a triple-q IC CDW forms that breaks translational symmetry but retains the surface point group symmetries of the undistorted phase [18,19]. The effects of the CDW on the bulk symmetries in this phase are not yet understood. On further cooling, at $T_{IC-NC} = 353\,K$ there is a weak first-order transition to an NC CDW phase where three vertical mirror plane symmetries are broken [17] and

*gedik@mit.edu

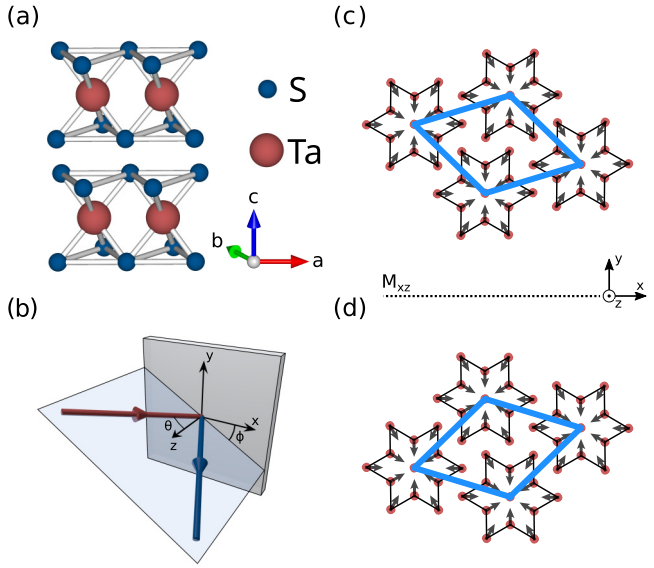

FIG. 1. (a) Structure of $1T$-TaS_2 in the undistorted phase. Ta and S atoms are depicted in red and blue, respectively. (b) Schematic of the experimental geometry. (c) ,(d) Structure of the CDW in the NC phase. Arrows denote the movement of the Ta atoms (red) below $T_{IC-NC} = 353$ K from their undistorted positions. The transition at T_{IC-NC} spontaneously breaks mirror symmetry, so that two different CDW configurations (α and β) can form, which have opposite planar chirality. The new unit cells of the two configurations are depicted in blue. M_{xz} denotes one vertical mirror plane which is broken beneath T_{IC-NC}. The others are related to M_{xz} by $\pm 120^\circ$ rotation about the z axis.

the surface point group becomes C_3. The NC phase has been visualized with scanning tunneling microscopy and exhibits patches of commensurate "Star of David" hexagrams that are separated by a network of discommensurations [20]. Because mirror symmetry is broken, there are two energetically equivalent CDW configurations (α and β) in the NC phase that have opposite planar chirality [Figs. 1(c) and 1(d)]. At even lower temperatures, $T_{NC-C} = 184$ K, $1T$-TaS_2 undergoes a symmetry-preserving first-order transition, where the discommensurations disappear and the CDW locks into a structure commensurate with the underlying lattice [21].

Recent interest in the NC phase of $1T$-TaS_2 has arisen due to the possibility of injecting mirror-opposite domains into the CDW structure [16], which do not otherwise develop during the IC-NC transition. Zong *et al.* were able to induce these domains using a single ultrafast pulse of light, which was found to drive the material into a long-lived metastable state possessing domains of opposite planar chirality. Partly motivated by the desire to image these domains, we seek here a simple experimental method that could identify domains with opposite planar chirality.

$1T$-TaS_2 samples used in the experiment were grown using the chemical vapor transport technique, as described in Ref. [16]. We verified that the NC phase of $1T$-TaS_2 was single-domain by performing electron diffraction on a sample from the same batch [22]. This is in agreement with previous work [15,16,23,24].

In RA-SHG [25–28], a pulsed laser beam of frequency ω and amplitude $E(\omega)$ is focused onto a sample with nonzero angle of incidence θ [Fig. 1(b)]. The 2ω component of the radiation emitted by the sample is subsequently measured in various combinations of incoming and outgoing polarizations [either parallel (P) or perpendicular (S) to the plane of incidence] and as a function of the angle ϕ between the plane of incidence and some crystallographic axis. In noncentrosymmetric materials, the response is dominated by the bulk electric dipole moment $P_i(2\omega) = \chi_{ijk} E_j(\omega) E_k(\omega)$ [29], where χ_{ijk} is a material-specific susceptibility tensor that must be invariant under all symmetry operations present in the crystallographic point group. In centrosymmetric crystals such as $1T$-TaS_2, the bulk electric dipole response is forbidden [29,30]. In this case, the dominant response often comes from the surface of the sample, which necessarily breaks inversion symmetry [31]. SHG from surfaces of materials is described by a different susceptibility tensor, χ^S_{ijk}, which is constrained by the crystal symmetries of the surface. In addition, there can be bulk contributions from higher-order processes that are allowed in the presence of inversion symmetry, such as the bulk quadrupole response $Q_{ij}(2\omega) = \chi^Q_{ijkl} E_k(\omega) E_l(\omega)$ [13,32]. Our experimental implementation uses a fast-rotation setup similar to that described in Refs. [25] and [33]. Here, we use an 800-nm (1.55 eV) laser beam incident at 10° with respect to the (001) sample normal. Further experimental details can be found in the Supplemental Material [22].

To show that we are sensitive to the breaking of mirror symmetry across the IC to NC transition, we took RA-SHG data on $1T$-TaS_2 in both phases. Figures 2(a) and 2(b) show the second harmonic response from the sample above and below $T_{IC-NC} = 353$ K in two polarization channels, plotted as a function of ϕ. We are able to fit the rotational anisotropy in the IC phase using the surface point group C_{3v} [Fig. 2(a)], which is in agreement with previous reports [18,19]. It should be noted that in order to fit the S_{in}-S_{out} polarization channel appropriately, we find that it is necessary to add an additional bulk quadrupole contribution to the signal. The consequences of this contribution will be discussed later, but at the moment they do not affect our conclusions.

Upon cooling into the NC phase, mirror symmetry is spontaneously broken and the surface point group reduces to C_3 [17]. As a result, the RA-SHG exhibits a marked lowering of symmetry [Fig. 2(b)]. This lowering of symmetry can be understood by noting that the ϕ dependence of $I_{PS}(2\omega)$ under C_3 is given by [22]

$$I_{PS}(2\omega) = (A_0 + A_1 \cos(3\phi) + A_2 \sin(3\phi))^2, \quad (1)$$

where A_0, A_1, and A_2 are functions of the susceptibility elements χ^S_{ijk}.

Symmetry considerations [22] show that A_0 and A_1 vanish identically in the presence of mirror symmetry. The absence of these terms lead to the sixfold symmetry in the P_{in}-S_{out} channel and its alignment with the crystallographic axes as seen in Fig. 2(a). However, these terms can adopt nonzero values when mirror symmetry is broken. Below T_{IC-NC}, the RA-SHG intensity therefore exhibits a threefold rather than sixfold symmetric pattern, arising from a nonzero A_0. The

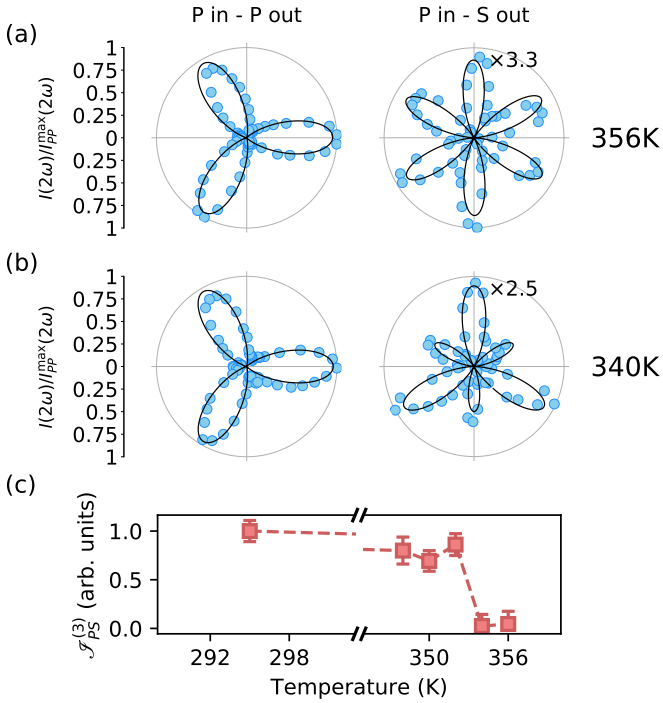

FIG. 2. (a), (b) Second harmonic intensity from 1T-TaS_2 as a function of ϕ above (a) and below (b) $T_{IC-NC} = 353$ K. For clarity, only two polarization channels are shown; the others are reproduced in the Supplemental Material [22]. Solid lines in (a) and (b) are best fits to the data using the surface point groups C_{3v} and C_3, respectively. Data is normalized to the maximum value of the P_{in}-P_{out} signal for each temperature. (c) Temperature dependence of the third Fourier coefficient, $\mathcal{I}_{PS}^{(3)}$, of the intensity (see main text and Supplemental Material [22] for details).

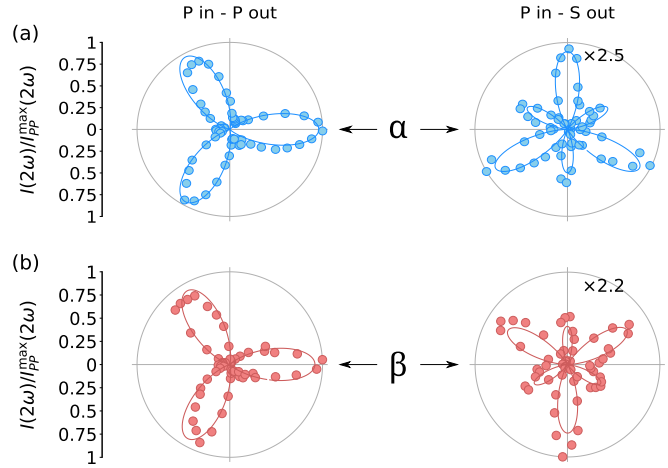

FIG. 3. Second harmonic intensity as a function of ϕ from mirror-opposite samples of 1T-TaS_2 in the NC phase ($T = 340$ K). The labels α and β refer to the two degenerate mirror-image configurations which are allowed in the NC phase. The solid line in (a) is a fit to the data using the surface point group C_3. The fit in (b) was generated by performing a mirror operation [22] to the numerical susceptibility tensor obtained from (a). Data is normalized to the maximum value in the P_{in}-P_{out} polarization channel for each sample.

effect of a nonzero A_1 is to rotate the RA-SHG intensity away from the high-symmetry axes, but we observe this coefficient to be zero within the resolution of our instrument. A negligible rotation of the SHG pattern should be expected, as the atomic positions of the Ta atoms only contract towards a central Ta atom and do not rotate away from their high symmetry axes to break the mirror symmetry [see Fig. 1(c) and 1(d)].

The three-fold nature of the RA-SHG intensity can be quantified experimentally by performing a spectral (sine) decomposition of the intensity and extracting the third Fourier coefficient, $\mathcal{I}_{PS}^{(3)}$, of $I_{PS}(2\omega)$ [22]. Figure 2(c) shows that $\mathcal{I}_{PS}^{(3)}$ appears discontinuously below T_{IC-NC}, consistent with the first-order nature of the phase transition. Taken together, the above considerations confirm that $\mathcal{I}_{PS}^{(3)}$ is a binary indicator of broken mirror symmetry in 1T-TaS_2.

Having established that RA-SHG is sensitive to the breaking of vertical mirror plane symmetry in 1T-TaS_2, we now seek to demonstrate that it can differentiate between CDW configurations of opposite planar chirality in the NC phase. To do so, we generate two samples with opposite planar chirality by cleaving a single sample of 1T-TaS_2. We then perform RA-SHG on both sides of the same cleave. Referring to Figs. 1(c) and 1(d), cleaving the sample is equivalent to performing a 180° rotation about the x-axis, which in a single layer is equivalent to a mirror reflection about M_{xz}.

Figure 3 shows the results of RA-SHG measurements in the P_{in}-P_{out} and P_{in}-S_{out} polarization channels as functions of ϕ, where the two mirror images are labeled α and β. As shown in the figure, whether the CDW configuration was α or β is indicated in RA-SHG by the orientation (up or down) of the pattern in the P_{in}-S_{out} channel, which is determined by the sign of A_0 in Eq. 1 [22]. This feature constitutes an experimental observable capable of identifying the sense associated with broken mirror symmetry in 1T-TaS_2.

To validate the analysis contained above, we first fit the data for the α structure using the surface point group C_3 to generate a tensor χ_{ijk}^{α} with numerical coefficients. The fit is shown in Fig. 3(a). Then, we transform χ_{ijk}^{α} by a mirror reflection about M_{xz} to generate χ_{ijk}^{β}[22]; with this transformation, we find that the rotational anisotropy simulated using χ_{ijk}^{β} collapses onto the measured signal, as shown in Fig. 3(b).

While the data contained in this work is specific to 1T-TaS_2, the analysis is applicable to a variety of different phase transitions involving broken mirror symmetry. By understanding which Fourier coefficients of the SHG intensity adopt nonzero values in the low-symmetry phase, one can show that almost every structural phase transition involving broken mirror symmetry implies a measurable change in the symmetry of the SHG pattern (i.e., beyond a simple change in overall intensity). We have performed a symmetry analysis of all possible phase transitions involving spontaneously broken mirror symmetry and in each case identified the relevant experimental indicator(s). The results of this analysis can be found in the Supplemental Material [22].

The final observation of this work concerns the contribution from the bulk of the sample to the measured RA-SHG signal. As mentioned above, we find that in order to fit the data in the S_{in}-S_{out} polarization channel correctly, we need to introduce an additional bulk quadrupole contribution to the

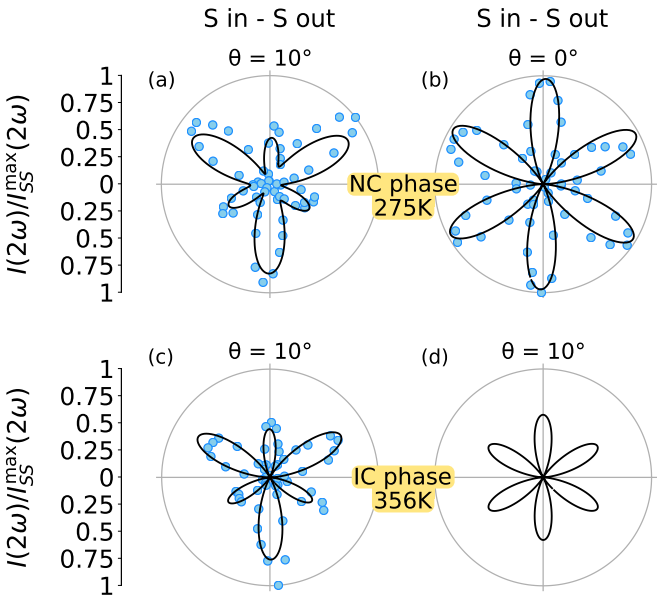

FIG. 4. Second harmonic intensity as a function of ϕ in the S_{in}-S_{out} polarization channel. Temperatures, phases, and incident angles (θ) are indicated in the figure. Also shown are fitting curves using the point group assignments (a) C_3 surface and S_6 bulk, (b) C_3 surface and S_6 bulk, (c) C_{3v} surface and S_6 bulk. (d) Best fit to data in (c) using C_{3v} surface and D_{3d} bulk. Data in all plots was normalized to one for clarity. Other polarization channels are depicted in the Supplemental Material [22].

SHG signal. This contribution, which is described by the effective polarization $\nabla_j Q_{ij} = 2i\chi^Q_{ijkl} k_j E_k E_l$, is the next-lowest order contribution to SHG and is allowed in the presence of inversion symmetry [13,32]. Importantly, the quadrupole contribution is generated by the entire illumination volume and is therefore insensitive to the surface symmetry. Quadrupole SHG can be identified by examining the θ dependence of the SHG intensity in the S_{in}-S_{out} channel. For purely electric dipole SHG, the symmetry in this channel does not depend on the incident angle. The θ dependence depicted in Figs. 4(a) and 4(b) therefore establishes the presence of a quadrupole contribution in our signal.

According to diffraction measurements [19], the correct surface and bulk point groups in the NC phase are C_3 and S_6, respectively. Figure 4(a) shows our results in this phase, which are consistent with this assignment. To understand the threefold symmetry in Fig. 4(a), we note that the ϕ dependence of $I_{SS}(2\omega)$ in this symmetry assignment is given by [22]

$$I_{SS}(2\omega) = (B_0 + B_1 \cos(3\phi) + B_2 \sin(3\phi))^2, \qquad (2)$$

where B_1 and B_2 are functions of the susceptibility elements χ^S_{ijk} and χ^Q_{ijkl}, but B_0 depends on χ^Q_{ijkl} only (and is zero when the quadrupole contribution is ignored). B_0 is then a probe of the bulk structure only and is not affected by the surface symmetry. When mirror symmetry is broken, all three coefficients are allowed and the function is threefold symmetric as in Fig. 4(a).

However, symmetry considerations [22] show that B_0 is zero in the presence of mirror symmetry. If bulk mirror symmetry were fully restored in the IC phase, we would therefore expect the signal to be sixfold symmetric. Figures 4(c) shows that the RA-SHG instead remains threefold symmetric in this phase, suggesting that the bulk breaks mirror symmetry. On the other hand, the highest-symmetry surface point group consistent with Figs. 2(a) and 4(c) is C_{3v}, which retains mirror symmetry. With RA-SHG, it is not possible to deduce the full crystal structure, but we speculate that this discrepancy between surface and bulk symmetries might be attributable to the particular stacking arrangement associated with the CDW above T_{IC-NC} [22]. This would explain why the surface component, which is measuring the local structure at the surface of the sample [31], is consistent with the existence of mirror symmetry, whereas the bulk component, which measures the global structure of many layers, is not.

In summary, we have demonstrated here that RA-SHG can be used to identify broken mirror symmetry in crystalline materials. In addition, we have found that RA-SHG can differentiate between structural configurations related by mirror reflection. By considering the different symmetry constraints on the S_{in}-S_{out} channel, we have also shown that RA-SHG is sensitive to broken mirror symmetry in the bulk of $1T$-TaS_2, and have found evidence that the IC phase of this material breaks mirror symmetry in the bulk. Importantly, our analysis is generalizable beyond the specific case of $1T$-TaS_2, and therefore opens up the possiblity for RA-SHG to detect mirror symmetry-broken phases and their domain structures in other candidate materials.

We would like to thank A. Po and L. Fu for helpful discussions regarding this work. This work was supported by the Gordon and Betty Moore Foundation's EPiQS Initiative Grant No. GBMF4540 to N.G. (data analysis and manuscript writing) and Grant No. GBMF3848 to J.G.C. (instrumentation), Shell through the MIT Energy Initiative (experimental setup and material development), and through DARPA DSO under DRINQS program Grant No. D18AC00014 (sample growth and data taking). L.Y. acknowledges support by the STC Center for Integrated Quantum Materials, NSF Grant No. DMR-1231319 and by the Tsinghua Education Foundation. B.G. gratefully acknowledges the German Academic Exchange Service (DAAD) for supporting his research stay with a fellowship.

[1] J. Sethna, *Statistical Mechanics: Entropy, Order Parameters, and Complexity* (Oxford University Press, Oxford, 2006).

[2] D. Thouless, *Topological Quantum Numbers in Nonrelativistic Physics* (World Scientific, Singapore, 1998).

[3] V. Belinicher and B. Sturman, Sov. Phys. Usp. **23**, 199 (1980).

[4] J. C. Y. Teo, L. Fu, and C. L. Kane, Phys. Rev. B **78**, 045426 (2008).

[5] T. H. Hsieh, H. Lin, J. Liu, W. Duan, A. Bansil, and L. Fu, Nat. Commun. **3**, 982 (2012).
[6] L. Fu, Phys. Rev. Lett. **106**, 106802 (2011).
[7] P. Hlobil, A. V. Maharaj, P. Hosur, M. C. Shapiro, I. R. Fisher, and S. Raghu, Phys. Rev. B **92**, 035148 (2015).
[8] R. G. Leisure and F. Willis, J. Phys.: Condens. Matter **9**, 6001 (1997).
[9] A. Migliori, J. Sarrao, W. M. Visscher, T. Bell, M. Lei, Z. Fisk, and R. G. Leisure, Physica B: Condens. Matter **183**, 1 (1993).
[10] G. E. Bacon, *X-ray and Neutron Diffraction* (Elsevier, Amsterdam, 1966).
[11] D. L. Dorset, *Structural Electron Crystallography* (Springer Science & Business Media, Berlin, 2013).
[12] T. F. Heinz, M. M. T. Loy, and W. A. Thompson, Phys. Rev. Lett. **54**, 63 (1985).
[13] D. H. Torchinsky and D. Hsieh, in *Magnetic Characterization Techniques for Nanomaterials*, edited by C. S. Kumar (Springer, Berlin, 2017), pp. 1–40.
[14] J. W. Harter, Z. Y. Zhao, J.-Q. Yan, D. G. Mandrus, and D. Hsieh, Science **356**, 295 (2017).
[15] J. Wilson, F. Di Salvo, and S. Mahajan, Adv. Phys. **24**, 117 (1975).
[16] A. Zong, X. Shen, A. Kogar, L. Ye, C. Marks, D. Chowdhury, T. Rohwer, B. Freelon, S. Weathersby, R. Li, J. Yang, J. Checkelsky, X. Wang, and N. Gedik, Sci. Adv. **4**(10), eaau5501 (2018).
[17] A. Spijkerman, J. L. de Boer, A. Meetsma, G. A. Wiegers, and S. van Smaalen, Phys. Rev. B **56**, 13757 (1997).
[18] C. B. Scruby, P. M. Williams, and G. S. Parry, Philos. Mag. **31**, 255 (1975).
[19] K. Fung, J. Steeds, and J. Eades, Physica B+C **99**, 47 (1980).
[20] X. L. Wu and C. M. Lieber, Science **243**, 1703 (1989).
[21] T. Ishiguro and H. Sato, Phys. Rev. B **52**, 759 (1995).
[22] See Supplemental Material at http://link.aps.org/supplemental/10.1103/PhysRevB.101.241106 for complete derivations, further experimental details, and additional data.
[23] M. Bovet, D. Popović, F. Clerc, C. Koitzsch, U. Probst, E. Bucher, H. Berger, D. Naumović, and P. Aebi, Phys. Rev. B **69**, 125117 (2004).
[24] K. N. H. Shiba, in *Structural Phase Transitions in Layered Transition Metal Compounds*, edited by K. Motizuki (D. Reidel Publishing Company, Dordrecht, 1986), pp. 175–266.
[25] J. W. Harter, L. Niu, A. J. Woss, and D. Hsieh, Opt. Lett. **40**, 4671 (2015).
[26] B. Lu, J. D. Tran, and D. H. Torchinsky, Rev. Sci. Instrum. **90**, 053102 (2019).
[27] D. H. Torchinsky, H. Chu, L. Zhao, N. B. Perkins, Y. Sizyuk, T. Qi, G. Cao, and D. Hsieh, Phys. Rev. Lett. **114**, 096404 (2015).
[28] B. Lu and D. H. Torchinsky, Opt. Express **26**, 33192 (2018).
[29] R. Boyd, *Nonlinear Optics*, 3rd ed. (Academic, New York, 2008).
[30] R. C. Powell, *Symmetry, Group Theory, and the Physical Properties of Crystals*, 1st ed., Lecture Notes in Physics, Vol. 824 (Springer-Verlag, New York, 2010).
[31] N. Bloembergen, R. K. Chang, S. S. Jha, and C. H. Lee, Phys. Rev. **174**, 813 (1968).
[32] Y. Shen, *The Principles of Nonlinear Optics*, Pure & Applied Optics Series: 1-349 (Wiley, New York, 1984).
[33] D. H. Torchinsky, H. Chu, T. Qi, G. Cao, and D. Hsieh, Rev. Sci. Instrum. **85**, 083102 (2014).